Civil Engineering ETDs   Engineering ETDs

9-3-2013

Nighttime evapotranspiration in a semiarid climate using a hemispherical chamber

Jacob Collison

Follow this and additional works at: https://digitalrepository.unm.edu/ce_etds

Jacob W. Collison
Candidate

Civil Engineering
Department

This thesis is approved, and it is acceptable in quality and form for publication:

Approved by the Thesis Committee:

Mark Stone , Chairperson

Dianna Crilley

John Stormont

Nighttime Evapotranspiration in a Semiarid Climate

using a Hemispherical Chamber

by

JACOB W. COLLISON

B.S., CIVIL ENGINEERING, UNIVERSITY OF NEW MEXICO, 2011

THESIS

Submitted in Partial Fulfillment of the

Requirements for the Degree of

Master of Science

Civil Engineering

The University of New Mexico

Albuquerque, New Mexico

July, 2013

ii

Nighttime Evapotranspiration in a Semiarid Climate using a Hemispherical Chamber

by

Jacob W. Collison

B.S., Civil Engineering, University of New Mexico, 2011
M.S., Civil Engineering, University of New Mexico, 2013

Abstract

Nighttime evapotranspiration (ET_n) is typically underestimated, miscalculated or ignored when producing daily, seasonal, or annual evapotranspiration (ET) models using energy-balance and aerodynamic conceptual models, such as the Penman-Monteith ET equation. The objective of this study is to increase the understanding of ET_n contribution to daily ET (ET_{24}) sums by using a hemispherical chamber to measure ET_n on three separate nights in the spring, summer, and fall in eastern Bernalillo County, New Mexico, 2012; a semiarid region where annual potential ET losses exceed annual precipitation. The hemispherical chamber is equipped with high-accuracy relative humidity and temperature sensors that measure ET directly using the methods described in Stannard (1988). The hemispherical chamber measurements were used to calibrate a Penman-Monteith (PM) equation to better account for ET_n by incorporating separate stomatal conductance models for daytime and nighttime. The amount of ET_n measured on these three nights were estimated to be 25 percent of the total ET_{24} modeled from micrometeorological data. Results from this study suggest that the single stomatal conductance PM model underestimated daily ET, due to inaccurately modeling ET_n, which is equivalent to 132 mm over a growing season in a semiarid climate.

iii

Table of Contents

LIST OF FIGURES

LIST OF TABLES

LIST OF UNITS AND ABBREVIATIONS

°C	Degree Celsius
d	Day
J	Joule
kg	Kilogram
m	Meter
mm	Millimeter
Pa	Pascal
sec	Second
W	Watt
CE	Coefficient of efficiency (Nash and Sutcliffe, 1970)
C_p	Specific heat of air (1012.5 J kg^{-1} °C^{-1})
DOY	Day-Of-Year
e_s	Saturation vapor pressure (kPa)
ET	Evapotranspiration (mm d^{-1})
ET_{24}	Daily evapotranspiration (mm d^{-1})
ET_d	Daytime evapotranspiration (mm d^{-1})
ET_{eq}	Available surface energy equilibrium (W m^{-2})
ET_{imp}	Bulk atmospheric demand (W m^{-2})
ET_n	Nighttime evapotranspiration (mm d^{-1})
G	Soil heat flux (W m^{-2})
g_a	Aerodynamic conductance (m s^{-1})
g_c	Canopy conductance (m s^{-1})
g_e	Soil surface conductance (m s^{-1})
g_s	Stomatal conductance (m s^{-1})
g_{sDay}	Daytime stomatal conductance (m s^{-1})
$g_{sMaxDay}$	Daytime maximum stomatal conductance (m s^{-1})
$g_{sMaxNight}$	Nighttime maximum stomatal conductance (m s^{-1})
g_{sNight}	Nighttime stomatal conductance (m s^{-1})
LF	Leach-field
LAI	Leaf area index (unitless)
RH	Relative humidity (unitless)
R_n	Net radiation (W m^{-2})
ST	Surrounding terrain
T_a	Air temperature (°C)
T_d	Daytime transpiration (m s^{-1})
T_n	Nighttime transpiration (m s^{-1})
u	Wind speed (m s^{-1})
VPD	Vapor pressure deficit (kPa)
Δ	Slope of the saturation vapor pressure curve (kPa °C^{-1})
γ	Psychrometric constant (kPa °C^{-1})
λ	Latent heat of vaporization of water (2.45 MJ kg^{-1})
λE	Latent heat flux (W m^{-2})
ρ	Air density (kg m^{-3})
Ω	Plant-Atmosphere decoupling factor (unitless)

CHABTER 1
Introduction

In arid and semiarid climates the annual potential ET is greater than the annual

precipitation, which means ET is limited by the amount of available water. In order to

account for ET losses from vegetated areas (riparian zones and irrigated agriculture)

accurate ET models that incorporate ET_n need to be produced. In order to estimate the

water losses due to ET for a water budget is to create a model that describes ET losses by

using energy-balance and aerodynamic conceptual models to describe the system. One of

the more commonly accepted ET models is the Penman-Monteith (PM) ET model, which

has been widely accepted for accurately describing ET losses (Monteith, 1965). The Food

and Agriculture Organization of the United Nations uses a form of the PM as their

standard equation for modeling crop ET (Allen et al., 1998). Most ET model equations

assume that nighttime evapotranspiration ET_n is negligible, and ignore ET_n. The objective

of this study is to use portable hemispherical chamber measurements taken during the

night to increase the understanding of ET_n and the ability of the PM model to estimate

ET_n.

Previous Studies

Historically, ET_n has been mostly neglected in its contribution to ET_{24} when using

models that rely on solar radiation as the driving force for water vaporization. The

transpiration from stomata for many plant species was assumed to be negligible during

the night due to the lack of photosynthetically active radiation (Jarvis and Mansfield,

1981). However, recent studies in semiarid climates on C_3 and C_4 plant species (which

1

were used specifically because plants that fix four carbon [C_4] dioxides during glycolysis are best adapted for hot and dry environments) have found that nighttime stomatal conductance (g_{sNight}) has been recorded as high as 90 percent of daytime stomatal conductance (g_{sDay}) (Snyder et al., 2003; Caird et al., 2007).

The limited studies addressing ET_n have used various approaches to quantify ET_n. Snyder et al. (2003) used gas exchange measurements to determine nighttime transpiration (T_n) in 11 plant species and found that T_n exceeded 10 percent of daytime transpiration (T_d) in all 11 plants, with seven plants T_n exceeding 15 percent of T_d. Studies that used sap flow rates to determine T_n include (but are not limited to) the following: two kiwifruit vines (*Actinidia deliciosa*) and an apple tree (*Malus sylvestris*) showed sap flow rates as high as 30 and 15 percent, respectively, of daytime rates (Green et al., 1989); Rose gum tree (*Eucalyptus grandis)* showed T_n to be 5 percent of daily totals (Benyon, 1999); and, lastly, a study in the Brazilian savanna (Cerrado tree species) showed T_n to be 15 to 22 percent of ET_{24} (Bucci et al., 2004). Weighing lysimeters have shown ET_n contributed 8 percent of ET_{24} for alfalfa (*Medicago sativa L.*) in North Carolina by England (1963) and 7 to 21 percent in spring and 0 to 15 percent in summer in the central Great Plains by Rosenberg (1969). A multi-crop and multi-irrigation condition study was conducted by Tolk et al. (2006) using weighing lysimeters in a semiarid climate. The reported ratio of ET_n to ET_{24} for the irrigated alfalfa from two independent lysimeters was 6.5 and 7.2 percent whereas the ratio for the deficit irrigated cotton (*Gossypium hirsutum L*) was 6.1 percent and the fully irrigated cotton was 7.3 percent. The accumulated ET_{24} for the deficit irrigated and fully irrigated cotton was 425 mm and 620 mm, respectively. Lastly, they used a decoupling factor (Ω), posed by

2

McNaughton and Jarvis (1983), which separates the driving forces of ET into radiation (equilibrium, ET_{eq}) and atmospheric demand (imposed, ET_{imp}) components. The Ω showed that nearly all ET_n was the result of ET_{imp}, primarily vapor pressure deficit. Using the eddy correlation method, Sugita and Brutsaert (1991) reported that ET_n accounted for 8% of ET_{24} for tall grass prairie vegetation and the Bowen-ratio method was used to determine ET_n for an irrigated alfalfa field in a semiarid climate, which resulted in 1.7 to 14 percent of ET_{24} (Iritz and Lindroth, 1994).

Hemispherical Chamber ET Studies

Hemispherical chambers (chamber) are advantageous when determining ET_{24} for locations that do not have adequate fetch, such as domestic septic disposal fields (leach-field) (LF) and sparsely vegetated areas, to support eddy-covariance and Bowen-ratio energy-balance ET methods (Schuepp et al., 1990; Stannard, 1997). In order to produce accurate ET models for areas without adequate fetch, ET chambers are used to measure actual ET at these locations with the resulting ET measurements used to calibrate a PM equation. Stannard et al., 2010 used this method to model the amount of ET_{24} from a LF in Jefferson County, Colorado in order to determine the amount of ET losses produced by a LF. Methods described in Stannard et al., 2010 were adjusted for this study in order to determine the amount of ET_n.

A 2-year (January 1, 2011-December 31, 2012) ET study concurrent to this study was conducted by the U.S. Geological Survey (USGS) on a LF in Bernalillo County, New Mexico to quantify the amount of ET_{24} losses from a LF in order to determine the amount of recharge a LF produces (Crilley and Collison, 2012). Both of these studies

3

accounted for minor nighttime soil evaporation losses through a soil surface conductance model (g_e) [see Eq. (10)], but they both used influence functions to describe stomatal conductance (g_s) that were only valid during the daytime.

Purpose and scope

The objective of this study is to increase the understanding of ET_n contribution to ET_{24} by using a hemispherical chamber to measure actual ET on three separate nights in the spring (May 19), summer (July 14), and fall (September 15) in eastern Bernalillo County, New Mexico, 2012. Using micrometeorological data collected at the study area an ET model was produced using the PM equation. The PM equation was calibrated through the use of daytime and nighttime chamber ET measurements to produce separate g_s models for daytime (g_{sDay}) and nighttime (g_{sNight}). A PM equation modified by McNaughton and Jarvis (1983) was used to determine whether bulk atmospheric conditions and/or available surface energy controlled daytime ET (ET_d) and/or ET_n. Based on the controlling conditions a dual g_s component ET model was produced using the PM equation. This dual g_s component ET model more accurately described ET_n for the vegetated area, the LF, which can be related to riparian zones and irrigated agriculture. These vegetated areas are important criteria for water budgets. Improving model ET predictions in these areas can improve water budget estimations of ET losses and help manage limited water resources.

4

Chapter 2
Materials and Methods

Site description

The study site is on the eastern edge of Bernalillo County, New Mexico with an elevation of 2,110 meters (m). This site corresponds to Site A in Crilley and Collison (2012). The study site was chosen because of the concurrent study of LF recharge being done by the USGS (Crilley and Collison, 2012), which utilized similar instrumentation and methods as this study. The LF is located in a clearing with the nearest copse of large 2 to 3-m tall trees [oneseed juniper (*Juniperus monosperma*)] located 30-m away. The dimensions of the LF are 18.3-m long by 6.4-m wide with a total area of 117.1 m^2 (Fig. 1). The LF is part of a dosing septic system where domestic effluent is pumped from a septic tank to the LF and dosed to one of three subsurface perforated pipes that distribute the effluent lengthwise along the LF. The LF has three distribution lines (L1, L2, and L3) 0.3 m below the surface with the flushable ports located on the south end of the LF. Effluent is sequentially cycled through the three distribution lines on each subsequent dosing. A LF of this type can be compared to a sub-surface drip irrigation system used in some agricultural settings. The immediate area around the LF, the surrounding terrain (ST), was also included in this study in order to determine the contribution of ET_n for non-irrigated sparsely-vegetated locations.

5
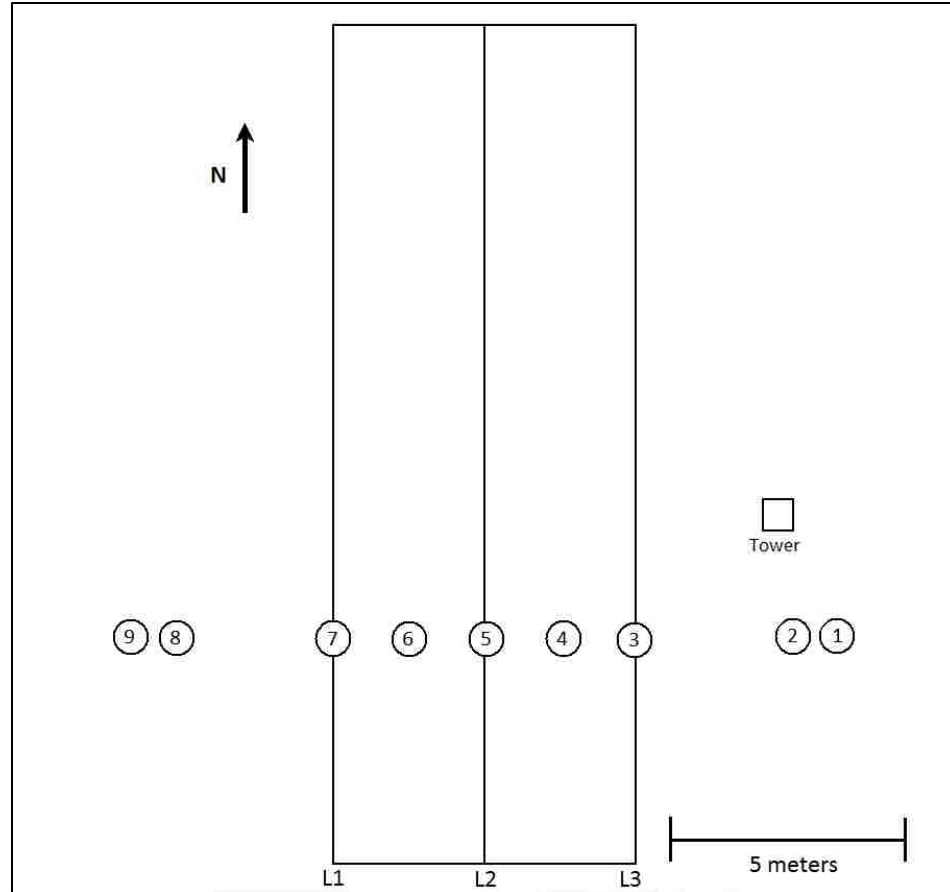
Fig. 1. Overhead to-scale drawing of study site. L1, L2, L3 correspond to perforated drain lines. The circles with numbers inside are the locations of chamber measurements, on the surrounding terrain (ST) and leach-field (LF), and the location of the weather station is noted as Tower

The ST was very sparsely-vegetated throughout the year, which is typical in semi-arid regions during years with limited precipitation. During the springtime, the vegetation that was dominant on the LF, based on photos and site visits, was blue grama (*Bouteloua gracilis*), a C_4 species, which would seed during early summer with Russian thistle (*Salsola kali* L.), also a C_4 species, becoming dominant during the monsoon season (late summer and through the fall). The ST vegetation throughout the year resembled that of the LF, but considerably less dense. The two distinct growing seasons, driven by snowmelt for the spring and the monsoon season for late summer and through the fall,

6

resulted in a bimodal leaf area index (one-sided green leaf area per unit ground surface area, LAI, unitless) curve (Fig. 2). The soil at this site consisted of 2-m thick of silty loam over a fractured limestone bedrock, which was determined from core samples taken by a truck mounted Geoprobe.
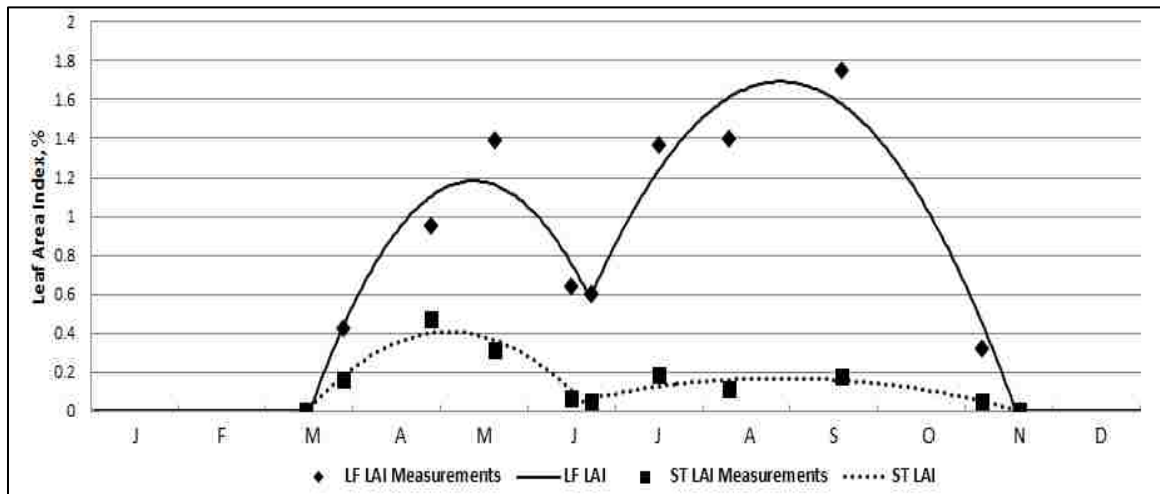
Fig. 2. Bimodal leaf area index (LAI) measurements and fitted curves for the leach-field (LF) and surrounding terrain (ST)

The climate at this site is characterized as Bsk – semiarid steppe (Peel et al., 2007). The 30-year (1981-2010) annual average from a nearby weather station is as follows: maximum temperature 17.1 degrees Celsius (ºC), minimum temperature 1.7 ºC, and precipitation of 480.8 millimeters (mm) (WRCC, 2013). During the 2-year study by Crilley and Collison (2012), the site had an average relative humidity of 40.8 percent and an average wind speed of 2.6 m s^{-1} (instrumentation height for wind speed is 2.8 m). The precipitation recorded during the study was 263 mm for 2011 and 162 mm for 2012 (D. Crilley, USGS, oral communication), which were both far below the 30-year average for the region.

7

Data collection

Micrometeorological measurements

      The micrometeorological data collected at this site is as follows: relative humidity, air temperature, barometric pressure, wind speed and direction, precipitation, net radiometer (on the LF and ST), soil temperature (on the LF and ST), soil heat flux (on the LF and ST), and soil water content (on the LF and ST). A 2.4-m tall weather tower was located 3 m to the east of the LF. The tower had a 2-m long pole that extended to the east (away from the LF) with a net radiometer attached to the end 1 m above the surface, allowing the sensor to measure net radiation, R_n (W m^{-2}), of the ST without interference of the LF. A steel pole was driven into the ground on the eastern edge of the LF and a 2-m long pole was extended horizontally to the surface to the west over the LF with a net radiometer attached to the end 1 m above the surface. The location of this net radiometer was where chamber measurement number 4 was taken (Fig. 1), but still in line with the weather tower. Below both net radiometers, soil-heat flux, G (W m^{-2}), soil temperature, T_s (ºC), and soil-water content, θ (m^3 water per m^{-3} soil), were measured. The weather tower measured variables common to both surfaces: wind speed (m s^{-1}), and wind direction at 2.8-m height, air temperature (ºC), and relative humidity (unitless) at 1.5 m height. Wind speed data was calculated as the average of the current time step (15 min) plus two time steps prior and two time steps after. This calculation was done to reduce the noise of high wind speed spikes and periods of little to no wind. Wet precipitation (mm) was measured with a tipping bucket attached to the pole on the eastern edge of the LF, except during winter months where precipitation was measured using a snowfall

8

adapter. Instrument sampling frequency was every 10 seconds and 15-min averages were recorded using a Campbell Scientific CR1000 data logger. Instrumentation types are as follows: temperature and relative humidity probe HMP50 by Vaisala, barometric pressure probe Barometer PTB110 by Vaisala, wind speed and direction by R.M. Young 05103, net radiation with a NR-LITE net radiometer by Kipp & Zonen, soil temperature with a TCAV- averaging soil thermocouple probe by Campbell Scientific, soil heat flux with a HFP01 heat flux sensor by Hukseflux, soil water content with a CS616 water content reflectometer by Campbell Scientific, and precipitation with a TE525 tipping bucket rain gage by Campbell Scientific. Installation and calibration of micrometeorological equipment followed manufacturer's instructions (D. Crilley, USGS, oral communication).

Hemispherical chamber

A portable hemispherical chamber (chamber) was used to measure direct ET on the LF and ST over the course of three nights in 2012: May 19, July 14, and September 15. These three nights were selected to represent three distinct seasons in a semi-arid climate. May 19 was chosen to measure ET_n during a typical springtime night before the dry-hot summer season started, with only 6.4 mm of precipitation in the prior month. July 14 was chosen to measure ET_n before the monsoon season started and after the typical dry-hot season, with only 2 mm of precipitation in the prior week. A rainfall event with 28.7 mm of precipitation occurred on July 5, which increased the soil water content (θ) on the LF from 18.6 to 29.7 percent and θ on the ST from 11.0 to 34.4 percent. By July 14 the θ had decreased to 21.9 and 22.6 percent for the LF and ST respectively. Lastly, September 15 was chosen to capture an ET_n measurement shortly after the monsoon

9

season, with 32.6 mm of precipitation in the prior month and 47 mm of precipitation

since the July 14 chamber measurement (Fig. 3).
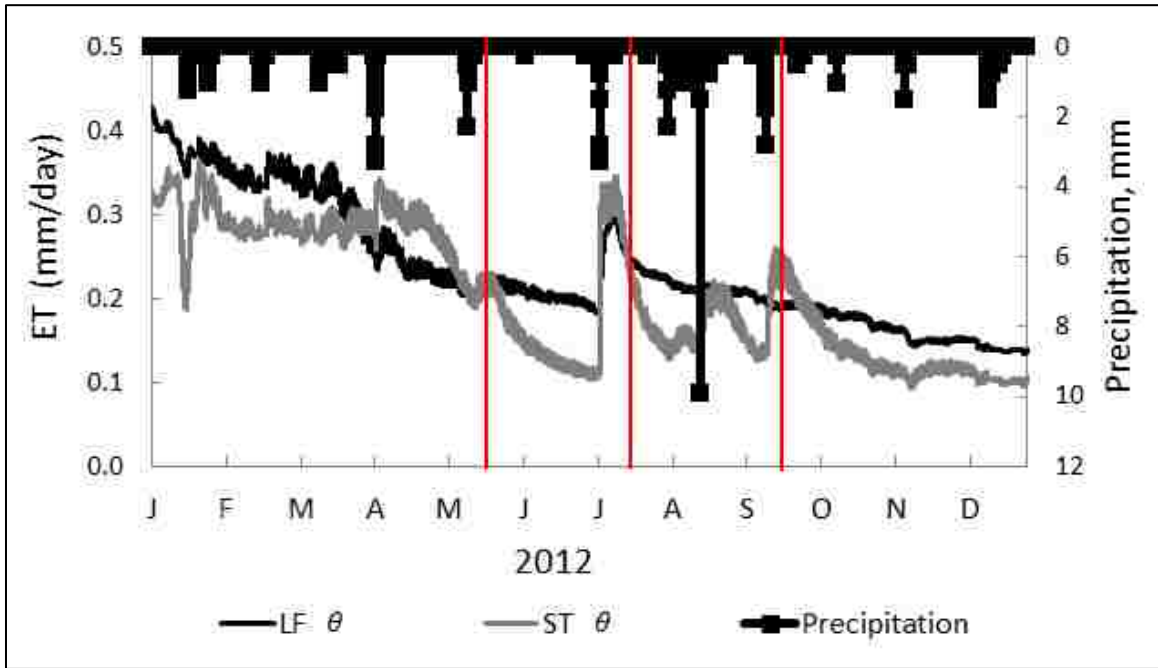
Fig. 3. Leach-field (LF) and surrounding terrain (ST) soil water content (θ) and precipitation (mm) for 2012 and nights of chamber measurements (vertical lines).

During the three nights when ET_n was measured with the chamber, the following

collection protocol was used: the chamber would be placed at a predetermined location

with sandbags hastily placed around the perimeter of the chamber to produce a good seal

with the ground surface, a high-accuracy relative humidity and temperature sensor would

collect data for two minutes at two second intervals at each location, and then the

chamber would be elevated off the ground to air out for one minute before the next

location. Measurements would begin at location 1 (Fig. 1) and proceed across the ST and

LF to end at location 9; this would be considered one run, with each run taking 30-mins

to complete. These locations were chosen in order to depict the LF and ST without being

biased based on vegetation locations. At the beginning of each run an average ambient

wind speed would be measured and the fans in the chamber would be adjusted

accordingly if needed. Measurement locations 1 and 2, and 8 and 9 were chosen to

represent the ST and were placed 3.3 m and 4.3 m off the eastern and western end of the

LF, respectively. ET_n measurements at ST locations were averaged to produce a single

ET_n value for a given run. Locations 3, 4, 5, 6, and 7 were chosen to represent the LF,

with locations 3, 5, and 7 conducted over each of the distribution lines and 4 and 6

between those lines. Locations 3, 5, and 7 typically had a higher ET_n than the

measurements between the lines. Measurements 3, 4, 5, 6, and 7 were averaged together

to produce one ET_n per run that was representative of the entire LF. During the three

nights that ET_n measurements were collected, 7 to 12 chamber runs were conducted over

7 to 13 hours (Table 1). May 19 measurements were cut short due to an instrument

malfunction. A discussion on chamber construction, calibration, use, and data processing

can be found in Stannard (1988), Stannard and Weltz (2006).

Table 1
Number of chamber runs during the three nights ET_n was measured and the number of
chamber measurements taken on the leach-field (LF) and surrounding terrain (ST).

Date	Number of chamber Runs	Before Sunset Measurements		Nighttime Measurements		After Sunrise Measurements	
		ST	LF	ST	LF	ST	LF
5/19/2012	7	12	15	16	20	--	--
7/14/2012	12	12	15	28	35	8	10
9/15/2012	7	4	5	16	20	8	10

Evapotranspiration modeling

The Penman-Monteith (PM) ET_{24} model (Monteith, 1965) utilizes both energy-balance and energy transfer to estimate ET_{24}. The accuracy of ET computed using the PM model can be further enhanced with actual ET measured using a chamber (Stannard et al., 2010; Crilley and Collison, 2012). The form of the PM equation used in this study is as follows:

$$\lambda E = \frac{\Delta(R_n - G) + g_a \rho C_p VPD}{\Delta + \gamma(1 + g_a/g_c)} \tag{1}$$

where λE is the latent-heat flux (W m^{-2}), Δ is the slope of the saturation vapor pressure curve (kPa °C^{-1}), R_n is net radiation (W m^{-2}), G is soil-heat flux (W m^{-2}), g_a is aerodynamic conductance (m s^{-1}), ρ is air density (kg m^{-3}), C_p is the specific heat of air (1012.5 J kg^{-1} °C^{-1}), VPD is vapor-pressure deficit (kPa), γ is the psychrometric constant (kPa °C^{-1}), g_c is the canopy conductance (m s^{-1}), and λ is the latent heat of vaporization of water (2.45 MJ kg^{-1}). The quantities of Δ, γ, g_a, and ρ were calculated using the procedures described in ASCE (2005), and VPD was calculated using Lowe's (1977) equation for saturation vapor pressure, e_s (kPa), in equation $(1-RH)e_s$, where RH is relative humidity (unitless).

McNaughton and Jarvis (1983) modified the PM equation in order to break the major components of the model into equilibrium ET (ET_{eq}) and imposed ET (ET_{imp}). The ET_{eq} component of the model is a function of available energy at the surface and the ET_{imp} component is a function of bulk atmospheric conditions. The modified PM equation is as follows:

$$\lambda E = \Omega \left[\frac{\Delta(R_n + G)}{\Delta + \gamma}\right] + (1 - \Omega)\left[\frac{g_c \rho C_p VPD}{\gamma}\right] \tag{2}$$

12

where Ω is the plant-atmosphere decoupling factor (unitless). The first half of Eq. (2) is the ET_{eq} and the second half is the ET_{imp}. The two parts of Eq. (2) are weighted by Ω, which is defined as:

$$\Omega = \left[1 + \left(\frac{\gamma}{\Delta+\gamma}\right)\left(\frac{g_a}{g_c}\right)\right]^{-1} \qquad (3)$$

Equation 2 is considered "decoupled" from bulk atmospheric conditions when Ω is near 1 and "coupled" when Ω is near zero. For example, during a sunny day the value of Ω will be near 1 and the bulk of the potential daily ET (ET_d) will be produced by the ET_{eq} portion of Eq. (2). Conversely during the night Ω will remain near zero and the bulk of ET_n will be produced by the ET_{imp} portion of Eq. (2).

The accuracy of a PM model is based on how well the behavior of g_c can be modeled. Stewart (1988) posed that g_c and g_s are proportionally related, as seen in the equation below:

$$g_c = g_{s(Day \ or \ Night)} * LAI \qquad (4)$$

With g_s being a very difficult quantity to measure and quantify g_s has been related to values more easily measured such as net radiation, vapor-pressure deficit, soil-water content, and time of day (Callander and Woodhead, 1981; Jarvis, 1976; Livingston and Black, 1987; Stewart, 1988; Stewart and Verma, 1992; Whitley et al., 2009). These variables are assumed to control g_s and each were fitted into influence functions, $f[\ ]$ (unitless), as compiled by Stannard et al. (2010) and used in Crilley and Collison (2012). These influence functions work in conjunction with each other and vary between 0 and 1 to control plant stomates, with the following form:

$$g_{sDay} = g_{smaxDay} * f[R_n] * f[\theta] * f[VPD] * f[t] \qquad (5)$$

13

where $g_{smaxDay}$ is the maximum value of g_s during the day, corresponding to fully open stomates. In order to determine g_c, Eq. (1) was set equal to the ET measured by the chamber. Using micrometeorological data associated with the time the chamber measurements were taken Eq. (1) was solved for g_c. The solved for values of g_c were then converted to g_s with Eq. (4). The g_s values calculated using chamber measurements were compared to those computed using the PM equation with influence functions modeling g_s. Nonlinear regression was used to reduce the difference between the modeled and measured g_c values by optimizing the coefficients in the R_n, θ, and VPD influence functions. The coefficients for the time of day influence function were selected by inspection, as explained in Stannard et al. (2010). Once these coefficients were optimized, the value for g_{smax} was selected by nonlinear regression to further reduce the difference between modeled and measured ET_{24} values. The influence function for R_n is as follows:

$$\mathfrak{f}[R_n] = \frac{(R_n-K)(R_{nmax}-K+C_1)}{(R_{nmax}-K)(R_n-K+C_1)} \tag{6}$$

where R_{nmax} is the maximum R_n value measured at the study site, 785 and 685 W m^{-2} for the LF and ST, respectively, K is the value of R_n as solar radiation goes to zero, -62 W m^{-2} for the LF and ST (Campbell, 1977; Stannard et al., 2010), and C_1 is a modeled parameter determined by nonlinear regression. The influence function for θ is as follows:

$$\mathfrak{f}[\theta] = \frac{1-exp^{(C_2*\theta_E)}}{1-exp^{C_2}} \tag{7a}$$

$$\theta_E = \frac{\theta-\theta_{wp}}{\theta_{fc}-\theta_{wp}} \tag{7b}$$

14

where θ_{wp} is the value of θ at wilting point (0.097), θ_{fc} is value of field capacity (0.331 and 0.281 for LF and ST respectively) (Stannard et al., 2010) and C_2 is a modeled parameter. The influence functions for VPD and t is as follows:

$$f[VPD] = exp^{(C_3*VPD)} \tag{8}$$

$$f[t] = 1 - C_4(t - C_5)^2 \tag{9}$$

where C_3 is a modeled parameter, C_4 and C_5 were selected by inspection and trial-and-error (Stannard et al., 2010).

Measuring Actual Evaporation

In order to determine actual evaporation from soil surface, sections of the LF and ST were treated with an herbicide to prevent vegetation from growing. These locations were measured periodically with the chamber in 2012 to calibrate a soil surface conductance model with the following equation (Stannard et al., 2012):

$$g_e = g_{emax} \left(\frac{1 - exp^{(C_2*\theta)}}{1 - exp^{C_2}} \right) \tag{10}$$

where g_e is a surface conductance (m s^{-1}) corresponding to the small contribution from soil evaporation, C_2 is assumed to be the same as used in $f[\theta]$ (Stannard et al., 2010), and g_{emax} was determined from regression using the chamber measurements over the non-vegetation areas of the LF and ST (Crilley and Collison, 2012). In Stannard et al. (2010) and in Crilley and Collison (2012), g_e was used to model ET_{24} when conditions inhibited transpiration, mainly during nighttime conditions, resulting in potential underestimation of ET_{24}. The PM model was set up to use the greater of g_c or g_e, unless the ground was

15

frozen and neither was used and ET was set to zero. The periods when $g_e > g_c$ typically happened during the nighttime.

Dual Stomatal Conductance Penman-Monteith Model

In order to quantify when ET_{eq} or ET_{imp} had a greater influence on ET, Eq. (2) was solved for ET_{eq} and ET_{imp} individually. A percent difference of ET_{eq} to ET_{imp} was taken, where negative percent differences related to a greater influence of ET_{eq} (day) on ET, and a positive percent difference related to greater influence of ET_{imp} (night) on ET. Equation (1) was modified to use two different g_s models; one for daytime (g_{sDay}) and one for nighttime (g_{sNight}), based on which component of Eq. (2) had the greater influence. The second g_s model is as follows:

$$g_{sNight} = g_{smaxNight} * f[\theta] * f[VPD] \tag{11}$$

where $g_{smaxNight}$ is the maximum g_s calculated using nighttime chamber measurements and following the same procedure used to calculate $g_{smaxDay}$. The influence functions for R_n and time of day were not used, since neither has an influence on ET_n.

When the percent difference of ET_{eq} to ET_{imp} was negative, the daytime g_s model, Eq. (5), was used to calculate the g_c that is used to calculate ET_{24} in Eq. (1). When the percent difference of ET_{eq} to ET_{imp} was greater than 1, the nighttime g_s model, Eq. (11), was used to calculate the g_c that is used to calculate ET_{24} using Eq. (1). During the transitional times at dawn and dusk, the controlling conditions of ET_{24} would shift from ET_{eq} to ET_{imp} and vice versa. During these transitions a weighted value of Eq. (2) using Eq. (5) would be added to a weighted value of Eq. (2) using Eq. (11), with the weighing

16

of each function determined by the percent difference of ET_{eq} to ET_{imp}. The percent difference values closer to 1 received more contribution from g_{sNight} model and values closer to 0 received more contribution from g_{sDay} model. Figure 4 below is a flowchart representation of the steps used to produce a dual g_s PM model.
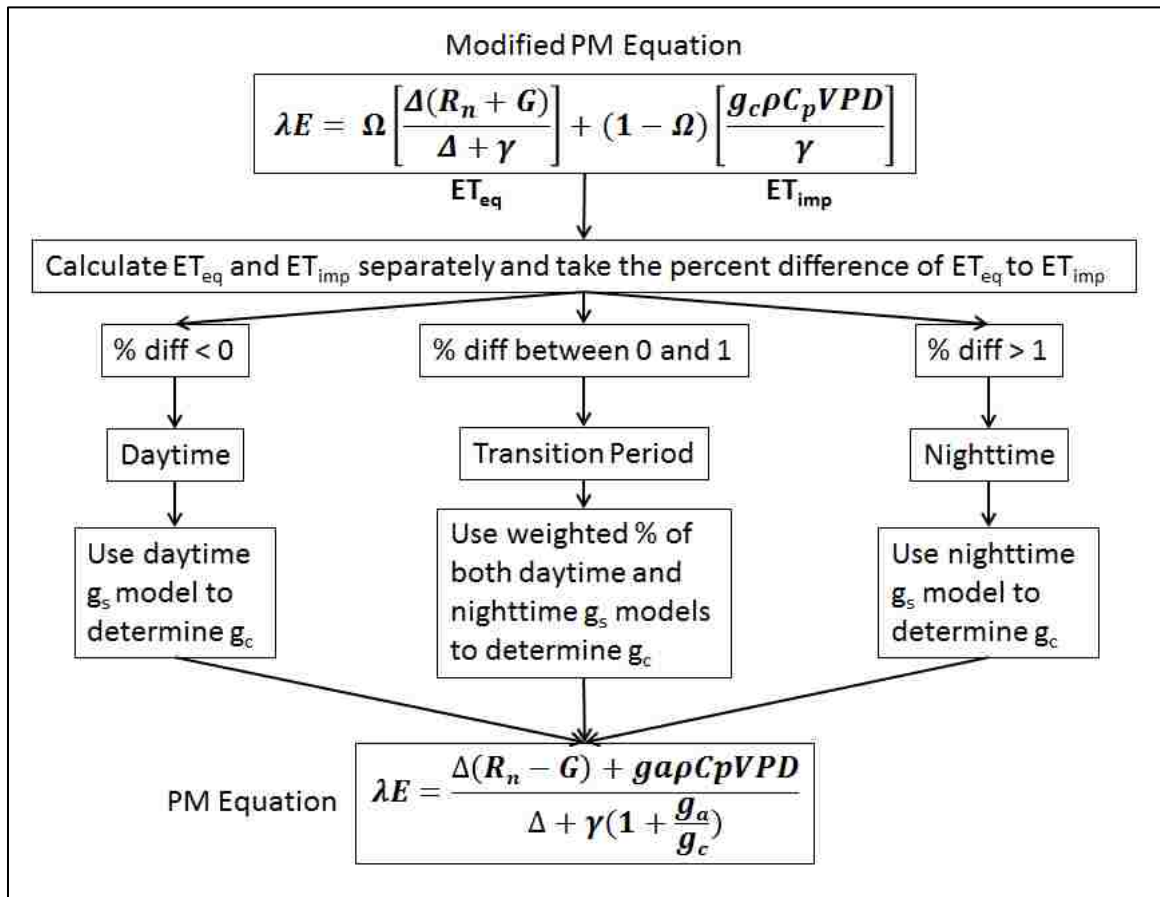
Fig. 4. Flowchart depicting the steps used to produce a dual stomatal conductance (g_s) Penman-Monteith (PM) model.

Chapter 3
Results

Nighttime chamber measurements

The results of nighttime chamber measurements taken on May 19, July 14, and

September 15, 2012 are shown in Fig. 5 and Table 2, with the raw data located in

Appendix A. Although May 19 ET_n measurements were cut short due to instrument

malfunction, it is reasonable to assume the ET_n values had approached a minimum value

based on the consistency of the last four measurements and a stable slope, similar to the

other two nighttime runs.
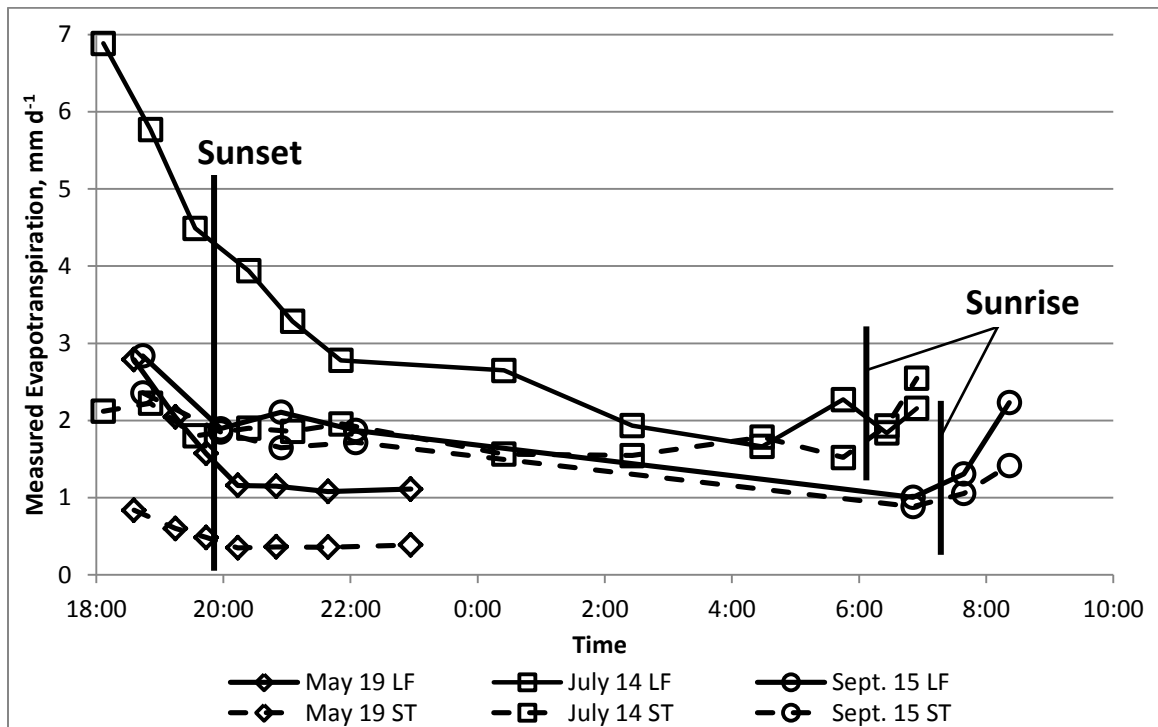
**Fig. 5. Averaged chamber measurements of evapotranspiration on three different
nights for leach-field (LF) and surrounding terrain (ST) with sunset and sunrise
shown.**

The night of July 14, 2012 had the greatest θ and VPD of all three nights on the LF and ST (Table 3). The lowest averaged ET measured during the three nights for the LF and ST respectively is as follows: 1.08 and 0.35 mm d^{-1} for May 19, 1.66 and 1.52 mm d^{-1} for July 14, and 1.00 and 0.88 mm d^{-1} for September 15 (Table 2). The ST on the night of July 14 had the lowest LAI of all three nights (Table 3), 0.13, but had the highest averaged ET_n for the ST, 1.73 mm d^{-1}, which suggests soil surface evaporation has a significant impact on ET_n. On the night of May 19, the amount of ET_n measured was the lowest of all three nights, even though that night had average micrometeorological and soil conditions compared to the other two nights, with the only major difference being it was the coldest night.

19

Table 2
Minimum, average, and maximum chamber measured ET_n values for the leach-field and surrounding terrain.

Date and Time, 2012 (MDT)	Leach-Field Measured ET (mm d^{-1})			Surrounding Terrain Measured ET (mm d^{-1})		
	Min.	Avg.	Max.	Min.	Avg.	Max.
5/19 18:35	1.92	2.79	5.32	0.73	0.84	0.99
5/19 19:14	1.43	2.04	3.95	0.35	0.60	0.84
5/19 19:43	1.13	1.57	2.64	0.28	0.48	0.61
5/19 20:13	0.80	1.16	1.88	0.21	0.35	0.45
5/19 20:49	0.75	1.15	1.73	0.18	0.36	0.55
5/19 21:38	0.65	1.08	1.67	0.19	0.36	0.51
5/19 22:56	0.83	1.11	1.57	0.17	0.39	0.49
7/14 18:06	3.57	6.89	8.52	1.63	2.12	2.51
7/14 18:51	3.99	5.77	7.42	2.09	2.22	2.32
7/14 19:33	3.74	4.49	5.45	0.99	1.80	2.28
7/14 20:23	3.36	3.94	4.78	1.43	1.90	2.26
7/14 21:05	2.80	3.28	3.60	1.39	1.86	2.09
7/14 21:50	2.31	2.78	3.17	1.59	1.96	2.33
7/15 00:24	2.41	2.65	2.86	1.28	1.56	1.78
7/15 02:25	1.34	1.93	2.93	1.04	1.54	1.91
7/15 04:28	1.25	1.66	2.35	1.46	1.78	2.06
7/15 05:45	1.52	2.27	3.46	0.91	1.52	1.90
7/15 06:26	1.19	1.84	3.09	1.19	1.93	2.47
7/15 06:54	1.45	2.16	3.83	1.55	2.55	3.24
9/15 18:43	2.23	2.84	4.36	2.11	2.36	2.63
9/15 19:57	1.38	1.89	2.24	1.70	1.85	2.02
9/15 20:54	1.76	2.11	2.43	1.38	1.65	1.82
9/15 22:04	1.48	1.87	2.32	1.51	1.72	1.88
9/16 06:50	0.75	1.00	1.29	0.75	0.88	0.99
9/16 07:38	0.76	1.31	1.83	0.85	1.05	1.33
9/16 08:21	1.74	2.23	2.65	0.92	1.42	1.89

Table 3

Averaged atmospheric and soil parameters during the three nights ET_n was measured and the LAI value for those nights. (VPD – Vapor pressure deficit, Temp – Air temperature, RH – Relative humidity, θ – Soil water content, LAI – Leaf area index, LF – Leach-field, ST – Surrounding terrain)

Date	Avg. VPD (kPa)	Avg. Air Temp. (°C)	Avg. RH (%)	Avg. Wind Speed (m s^{-1})	Avg. LF θ (%)	Avg. ST θ (%)	LF LAI (unitless)	ST LAI (unitless)
5/19/2012	0.92	12.1	47.1	1.9	21.43	21.54	1.15	0.36
7/14/2012	1.68	20.5	33.7	1.1	26.53	28.56	1.28	0.13
9/15/2012	0.98	13.7	39.5	2.1	19.16	22.68	1.55	0.16

On the night of May 19 the chamber measured a minimum ET_n value of 1.08 and 0.35 mm d^{-1} for the LF and ST respectively, which was 16 and 20 percent of the daytime maximum modeled ET_{24} for the prior day. Of the three nights, May 19 had the lowest LF LAI of 1.15, and the nighttime average of select atmospheric and soil variables are as follows: VPD was the lowest, RH was the highest, T_a was the lowest, and θ for the LF and ST was the median (Table 3).

On the night of July 14 the chamber measured a minimum ET_n value of 1.66 and 1.52 mm d^{-1} for LF and ST respectively, which was 14 and 58 percent of the daytime maximum modeled values for the LF and ST for the prior day. Of the three nights, July 14 had the median LF LAI of 1.28, and the nighttime average of the remaining key atmospheric and soil variables is as follows: VPD was the highest, RH was the lowest, T_a was the highest, and θ for the LF and ST was the highest (Table 3).

On the night of September 15 the chamber measured a minimum ET_n value of 1.00 and 0.88 (mm d^{-1}) for LF and ST respectively, which was 13 and 60 percent of the daytime maximum modeled values for the LF and ST for the prior day. Of the three nights, September 15 had the highest LF LAI of 1.55 and the nighttime average of the

21

remaining key atmospheric and soil variables is as follows: VPD was the median, RH was the median, T_a was the median, and θ for the LF and ST was the lowest (Table 3).

Evapotranspiration

Using a single g_s model within a PM model (Eq. 1), which uses g_e to approximate soil surface evaporation during the night, estimated that ET_n accounted for 5.8 and 17.1 percent of ET_{24} for LF and ST, respectively, between Day-Of-Year (DOY) 92 and 275. Using a dual g_s model within a PM model (Eq. 1) estimated that ET_n accounted for 25.1 and 26.0 percent of ET_{24} for LF and ST, respectively, during the same period. Figures 6, 7, and 8 below show the nighttime chamber measurements and how they relate to a single g_s PM model and dual g_s PM model.
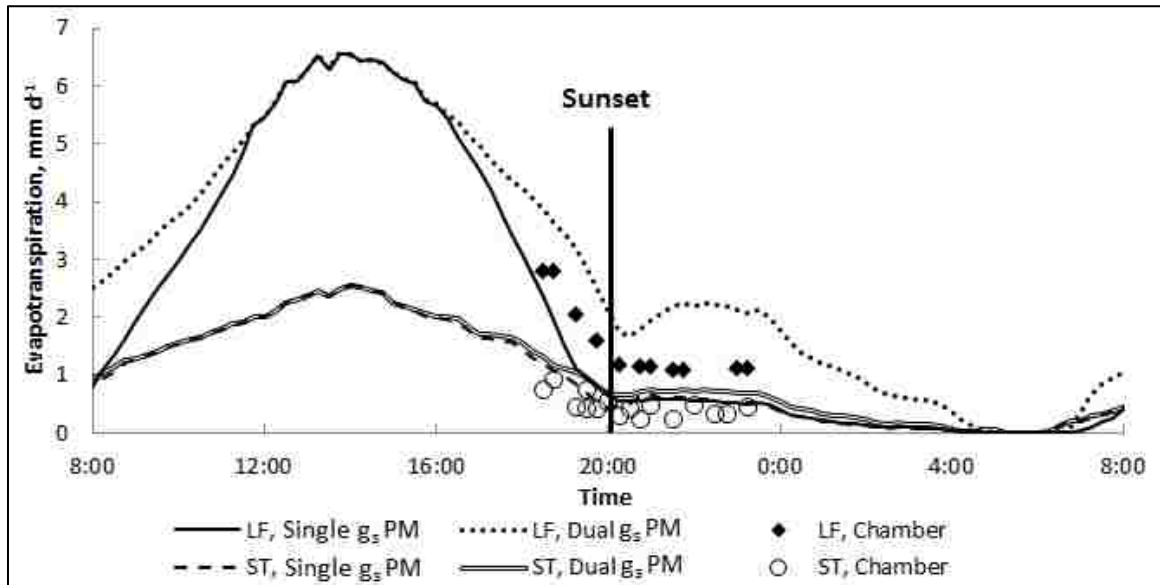
Fig. 6. Time series modeled ET24 and measured ETn for May 19, 2012, leach-field (LF), surrounding terrain (ST), Penman-Monteith (PM), and Dual stomatal conductance (gs) PM model.

The night of May 19, 2012 had the lowest ET_n measured and was coldest night of the three nights; all other micrometeorological and soil values were similar to the other nights, which suggests ET_n may be a function of T_a even though daytime ET was found to be unrelated to T_a (Stannard et al., 2010). The dual g_s PM model overestimated ET_n during the period of chamber measurements for the LF and the ST. The single g_s PM model underestimated ET_n for the LF and closely resembled ET_n for the ST. The decrease in ET_n estimated by the dual g_s PM model shortly after 20:00 was due to a period of little-to-no wind, which decreased the aerodynamic conductance.
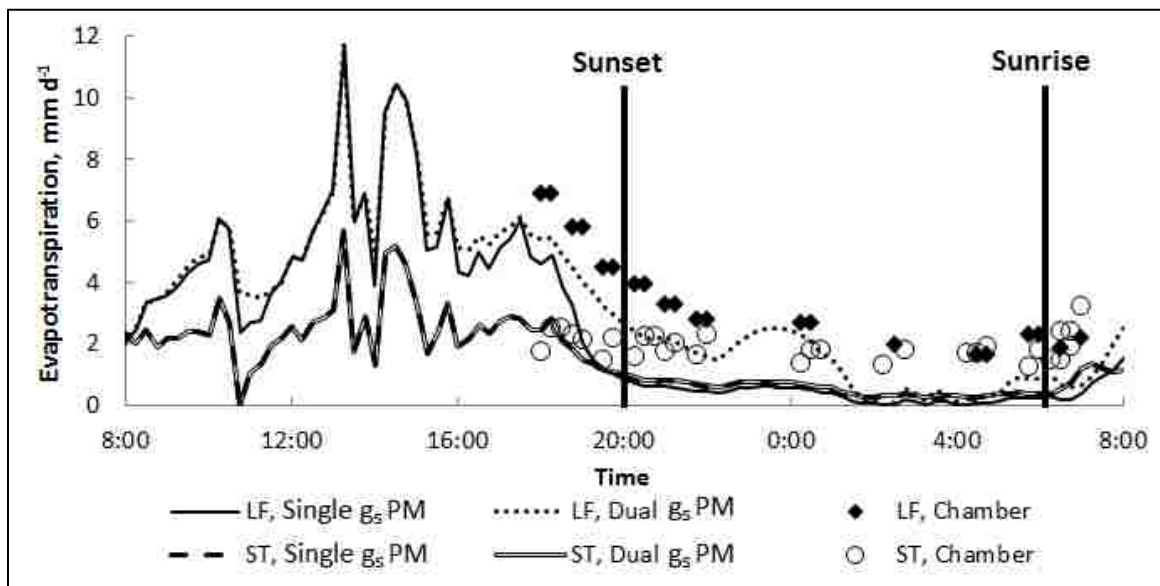
Fig. 7. Time series modeled ET24 and measured ETn for July 14, 2012, leach-field (LF), surrounding terrain (ST), Penman-Monteith (PM), and Dual stomatal conductance (gs) PM model. (ST, Single gs PM and ST, Dual gs PM are overlapped for the entirety of the plot).

On the night of July 14, 2012 the LF dual g_s PM model closely resembled chamber measurements of actual ET_n collected throughout the night, with the exception of around 4:00am, when there was a decrease in wind speed. Conversely, the ST dual g_s PM model was similar to the single g_s PM model for the entirety of the night. Both the single and dual g_s PM models underestimated ET_n for the ST throughout the night. July

14 had the greatest measured ET_n of all three nights. After midnight shortly after sunrise the chamber ET_n measurements for the LF and ST were very similar but the LAI for the LF was ten-times the value for the ST. This similarity in ET_n chamber measurements for the LF and ST and large difference in LAI values for the LF and ST suggests surface evaporation has a greater contribution to ET_n than Eq. (10) predicts. Condensation on leaves before sunrise was noticed during this night, which might explain the slight increase of ET measured by the chamber right before sunrise. The decrease in the dual g_s PM model from 2:00am to 5:00am was due to a period of little-to-no wind, which decreased aerodynamic conductance.
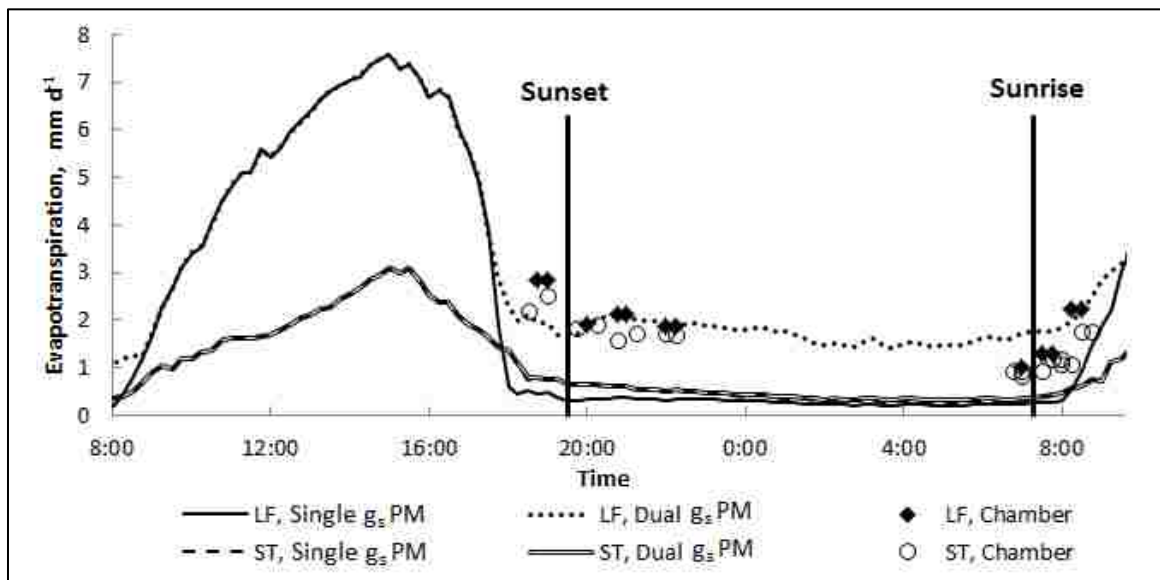
Fig. 8. Time series modeled ET24 and measured ETn for September 15, 2012, leach-field (LF), surrounding terrain (ST), Penman-Monteith (PM), and Dual stomatal conductance (gs) PM model. (ST, Single gs PM and ST, Dual gs PM are overlapped for the entirety of the plot).

On Sept. 15, 2012 the dual g_s PM model closely approximated actual measured ET_n for the LF throughout the night. The LAI for the LF and ST was 1.55 and 0.16 respectively. The measured ET_n for the LF and ST were similar throughout the night,

even though the LAI's were greatly different. This suggests that soil evaporation greatly contributes to ET_n. The dual g_s PM model for the ST closely resembled the single g_s PM model for the LF and ST throughout the night, all of which greatly underestimated the amount of ET_n. This underestimation is related to a small canopy conductance produced by Eq. (4) because of the small LAI of 0.16 for the ST. Wind speed was steady at 2 m s^{-1} throughout the night.

Both the single g_s PM models estimated a rapid decrease in ET a few hours before sunset and a rapid increase in ET within a few hours after sunrise for all three nights, whereas the actual ET_n measurements indicated a mild decrease and mild increase during those same periods. The dual g_s PM model for the LF estimated a mild decrease in ET a few hours before sunset and a mild increase in ET around sunrise.

A coefficient of efficiency (CE) was used to determine the goodness of fit and correlation between modeled and measured ET_n values. The CE has a range of $-\infty$ to 1, where 1 corresponds to a perfect match. CE values between 0 and 1 indicate model predictions accuracy; with values closer to 1 indicating more accurate predictions, and values closer to 0 indicating the observed mean is a better predictor than the model (Nash and Sutcliffe, 1970). The CE for the single g_s PM model for the LF and ST respectively are -0.73 and -0.96, which indicates the single g_s PM model poorly estimates ET_n. The CE for the dual g_s PM model for the LF had a CE of 0.47, indicating the dual g_s PM model for the LF produced fairly-accurate estimation of ET_n. Conversely, the dual g_s PM model for the ST had a CE similar to the single g_s PM model of -0.92, which indicates the dual g_s PM model poorly estimates ET_n.

Table 4

Evapotranspiration model coefficients and coefficient of efficiency (CE, Nash and Sutcliffe, 1970) for the single g_s Penman-Monteith (1 g_s PM), dual g_s Penman-Monteith (2 g_s PM) models, daytime maximum stomatal conductance ($g_{smaxDay}$), nighttime maximum stomatal conductance ($g_{smaxNight}$), and surface maximum conductance (g_{emax}).

Parameter	Leach-Field	Surrounding Terrain
C_1	112.88	73.95
C_2	-3.312	-4.321
C_3	-0.238	-0.098
C_4	0.014	0.014
C_5	14	14
g_{emax}	1.53E-03	1.33E-03
$g_{smaxDay}$ (m s^{-1})	4.99E-03	2.85E-03
$g_{smaxNight}$ (m s^{-1})	6.16E-03	3.53E-03
CE 1 g_s PM	-0.73	-0.96
CE 2 g_s PM	0.47	-0.92

Chapter 4
Discussion

The chamber measurements indicate that ET_n values decrease mildly before sunset and increase mildly after sunrise (Fig. 5, 6, 7, 8) for all three nighttime runs. The single g_s PM models estimate a more rapid decrease and increase before sunset and after sunrise. This rapid decrease and increase is related to the influence functions that describe net radiation and time of day for g_s. Using a PM model that uses a g_s model that does not include influence functions for net radiation and time of day more accurately estimated the mild decrease and increase of ET during the sunset and sunrise periods for on the LF. The dual g_s PM model for the ST did not correctly estimate the mild decrease and increase during the sunrise and sunset periods; instead this model closely resembles the single g_s PM models, which used g_e in place of g_c during the night to estimate ET_n. Since the value of LAI was considerably small for the ST, the value of g_c was typically less than the value of g_e during the night, which led the PM model to use g_e instead of g_c.

The ET_n value never reached zero, even on May 19, which had the lowest measured ET_n value of all three nights (0.35 mm d^{-1}). After the mild initial decrease in ET_n shortly before sunset, ET_n slowly and steadily decreased throughout the rest of the night, except for one measurement on the LF during the night of July 14, which showed a slight increase of ET_n right before the sunrise. This slight increase in ET_n corresponds with the observation of condensation on leaves before sunrise.

Stomatal conductance is a function of LAI with large values of LAI corresponding to large values of g_s and in turn large values of ET. The chamber ET measurements indicate that large LAI values are not always an indicator of large ET_n

27

values as shown by the measurements on July 14 and September 15. The night of July 14 had the smallest LAI (Table 3) on the ST of the three nights, but produced the largest ET_n measured on the ST. This contradiction of low LAI and high ET_n measurements leads to the assumption that there is other variable(s) contributing to ET_n. The night of July 14 had the highest average nighttime VPD and θ and the lowest average RH of all three nights. Air temperature also appeared to limit ET_n, as depicted by the May 19 measurements, with air temperature dropping to 4.9 °C during the night. The atmospheric conditions, soil conditions, and LAI were the median of the three nights on May 19 and yet the measured ET_n values were considerably lower than the other two nights (Fig. 5).

The chamber measurements on Sept. 15 for the LF and ST were extremely similar throughout the night, even though their LAI were drastically different, 1.55 vs. 0.15. This difference in LAI but very similar ET_n measurements further alludes to a larger controlling factor for ET_n than LAI and g_s. The dual g_s PM model accurately estimated Sept. 15 ET_n values throughout the night for the LF, which suggests the modeled g_{sNight} values were accurately modeling a conductance, but not g_s. The low LAI for the ST and high measured ET_n values for the ST suggests that the modeled g_s values for the LF and ST were accurately predicting soil surface conductance, evaporation.

During the computation to determine $g_{smaxNight}$ through nonlinear regression a new $g_{smaxNight}$ for the LF (0.00616) and ST (0.00353) was found that was greater than $g_{smaxDay}$ (Table 4). This new $g_{smaxNight}$ is unrealistic, due to the stomates being less conductive at night, but when considering the contribution of evaporation from the soil surface at night as being included in this new $g_{smaxNight}$, it becomes more reasonable. In order to more accurately estimate the contribution of nighttime transpiration and evaporation, a two-

28

component model, such as the Shuttleworth-Wallace model, would be required, which breaks transpiration and evaporation into separate components (Shuttleworth and Wallace, 1985).

The dual g_s PM model produced a decent goodness of fit CE value (0.47) only for the LF model, which is better than the CE for the single g_s PM model for the LF (-0.73) and ST (-0.96). The CE for the dual g_s PM model for the ST was similar in its inaccuracy to the single g_s PM model (-0.93) because of the how controlling LAI is on g_s.

Chapter 5
Conclusion

Using actual ET measurements through the use of a chamber on the nights of May 19, July 14, and September 15, 2012, a dual g_s PM model was established in order to determine the contribution of ET_n to ET_{24}. Two g_s models were created, one for the daytime and one for nighttime. Using a modified version of the PM equation, the controlling conditions for ET_d and ET_n was determined. The dual g_s PM model used these controlling conditions to determine when to use g_{sDay} or g_{sNight} models in estimating ET_{24}.

Using a dual g_s PM model has substantially increased the estimation of the contribution of ET_n to ET_{24} and increased the correlation between nighttime chamber measurements and modeled values on the LF. Using the dual g_s PM model the contribution of ET_n to ET_{24} was estimated to be 25 and 23 percent for the LF and ST, respectively, between DOY 92 and 275. Whereas using a single g_s PM model, the contribution of ET_n to ET_{24} for the LF and ST was estimated to be 9 and 19 percent, respectively, during the same time period. The contribution of ET_n to ET_{24} for the LF and ST during the nights of May 19, July 14, and September 15 was 29 and 28 percent, 23 and 21 percent, and 23 and 20 percent, respectively. Although the relationship between measured ET_n and modeled ET_n were not 1:1, substantial improvement for modeled ET_n were made by incorporating a second g_s model to calculate g_s for nighttime, which inadvertently included soil surface conductance.

The ST with its sparse vegetation cover does not model well during the night when using the dual g_s PM model. The PM model incorporates a big leaf assumption for the canopy, which becomes invalid for sparse vegetation cover (Stannard, 1993). Further

research is required to accurately model soil surface evaporation at night in order to produce a more accurate PM model for nighttime. A two-component model, Shuttleworth-Wallace model, should be investigated in order to separate the components of ET_n into transpiration and evaporation.

Results from this study indicate that ET losses from vegetated areas in a semiarid region can be greater than predicted when using single g_s component models. These vegetated areas (riparian zones and irrigated agriculture) are typically important contributions to water budgets. Improving model ET predictions in these areas can improve water budget estimations of ET losses and help manage limited water resources.

31

Appendices

Appendix A: Nighttime chamber measurement data and 2012 micrometeorological data used to make the model.

Appendix B: Micrometeorological and Soil plots for 24 h period spanning the nights when chamber data was collected.
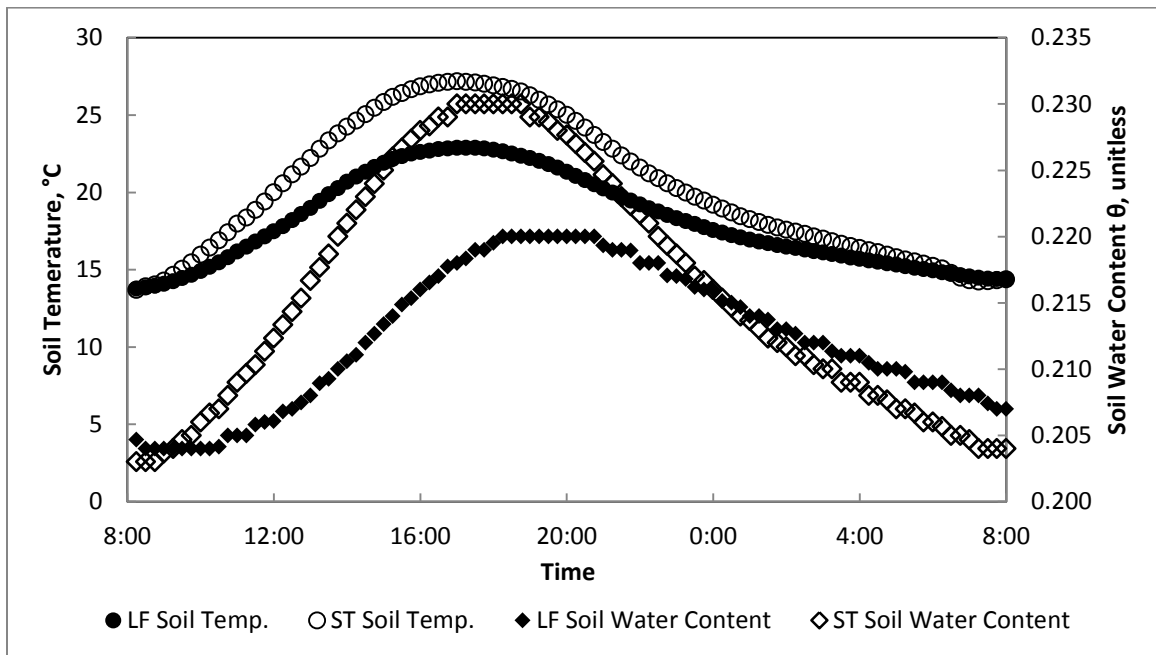
Appendix A
Nighttime chamber measurement data and 2012 micrometeorological data used to make the model.

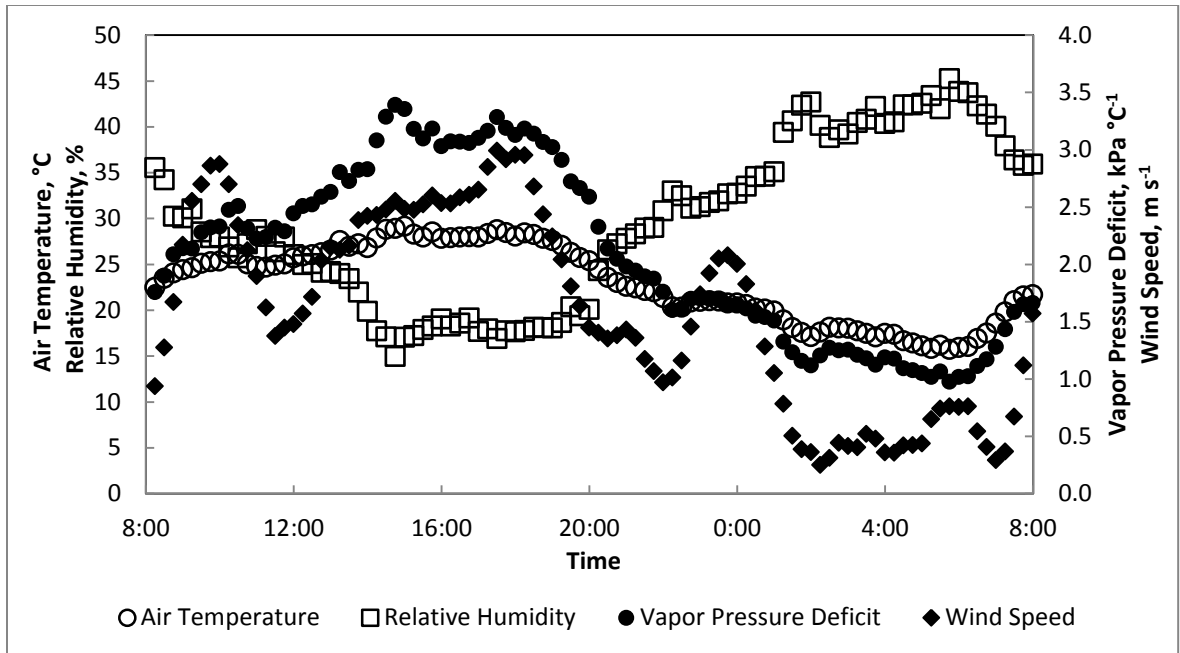**See Attached Supplemental data**

33

Appendix B
Micrometeorological and Soil Plots for 24 h period spanning the nights when chamber data was collected.
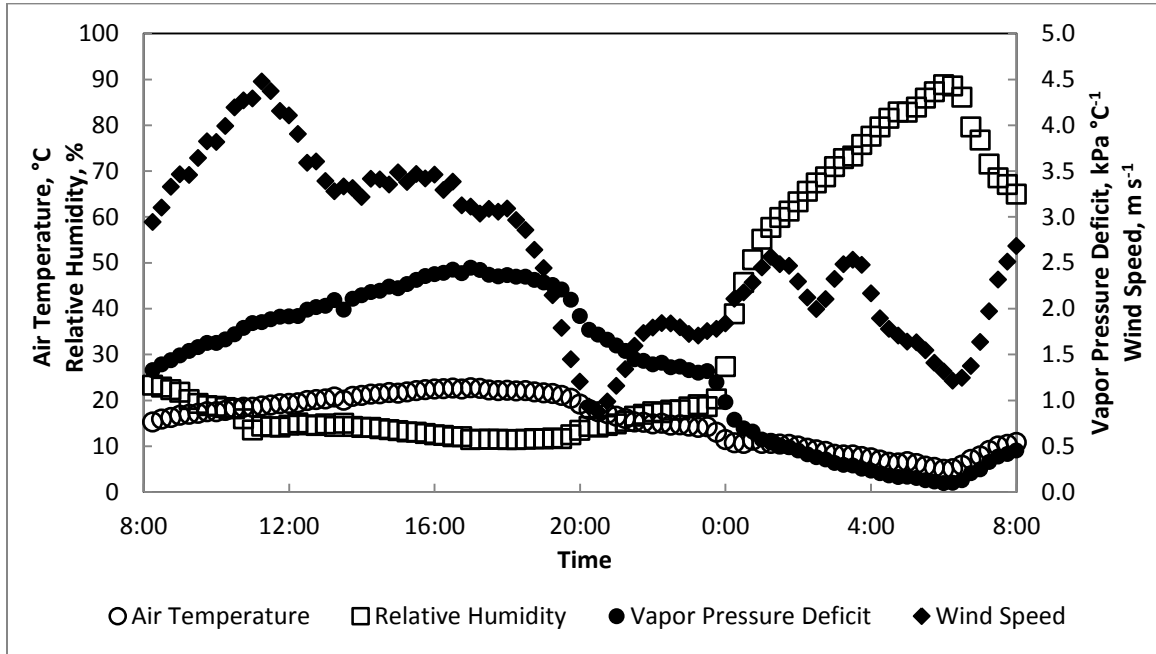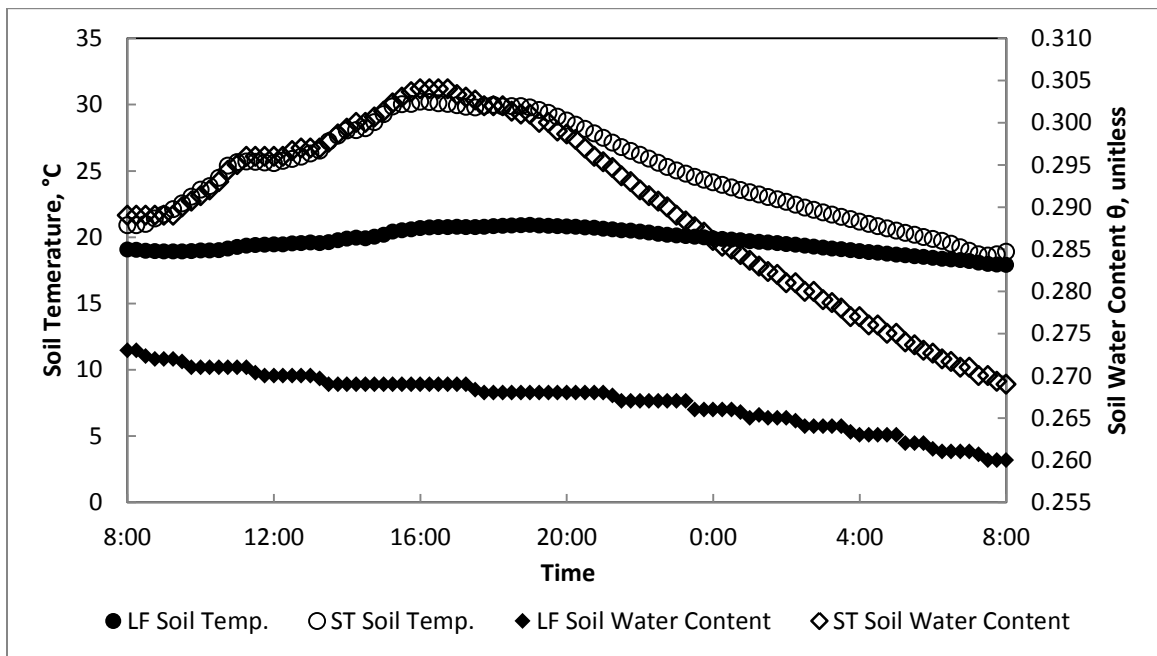

Fig. B1. Key atmospheric conditions spanning 8:00am May 19 to 8:00am May 20, 2012.
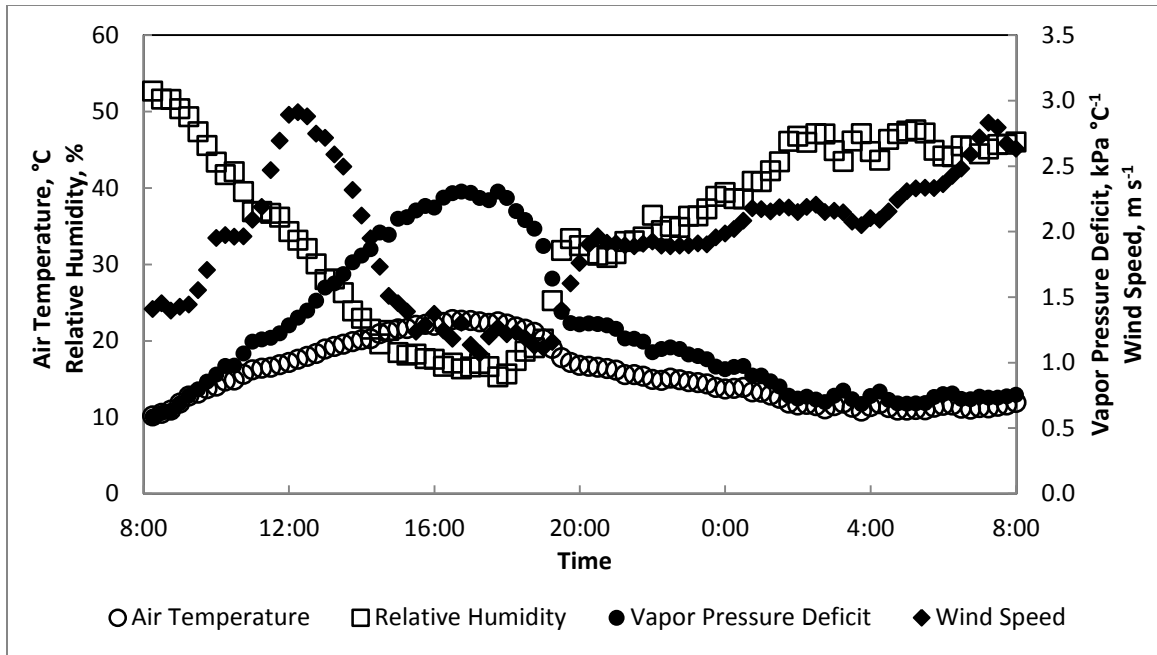

Fig. B2. Key soil conditions spanning 8:00am May 19 to 8:00am May 20, 2012.
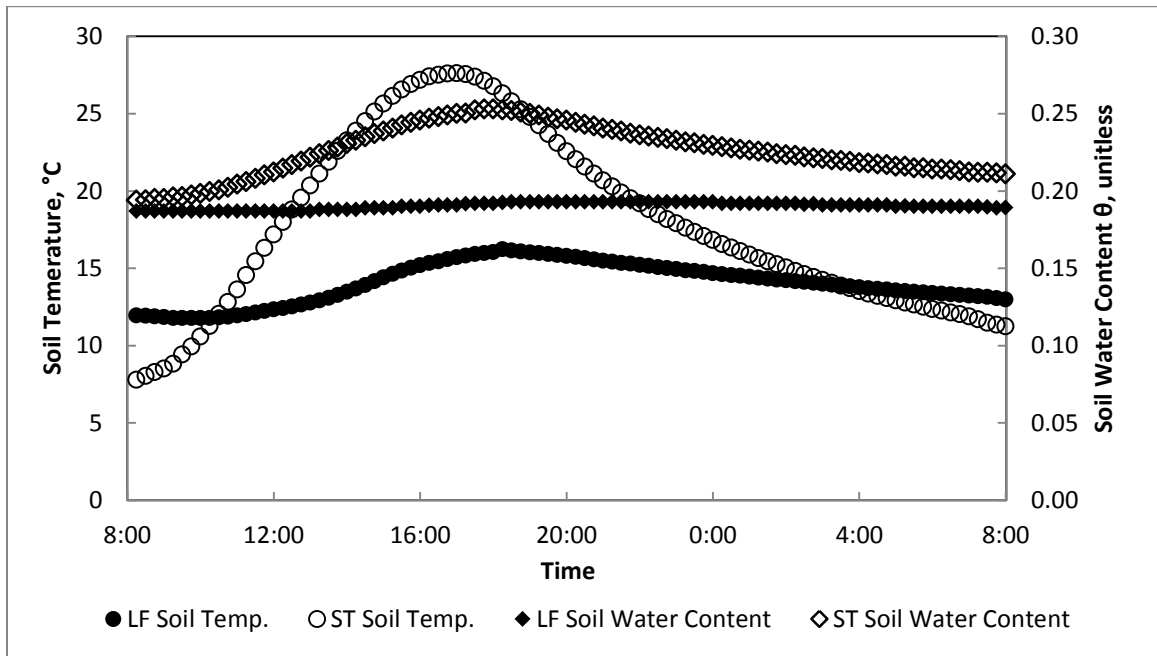
Fig. B3. Key atmospheric conditions spanning 8:00am July 14 to 8:00am July 15, 2012.
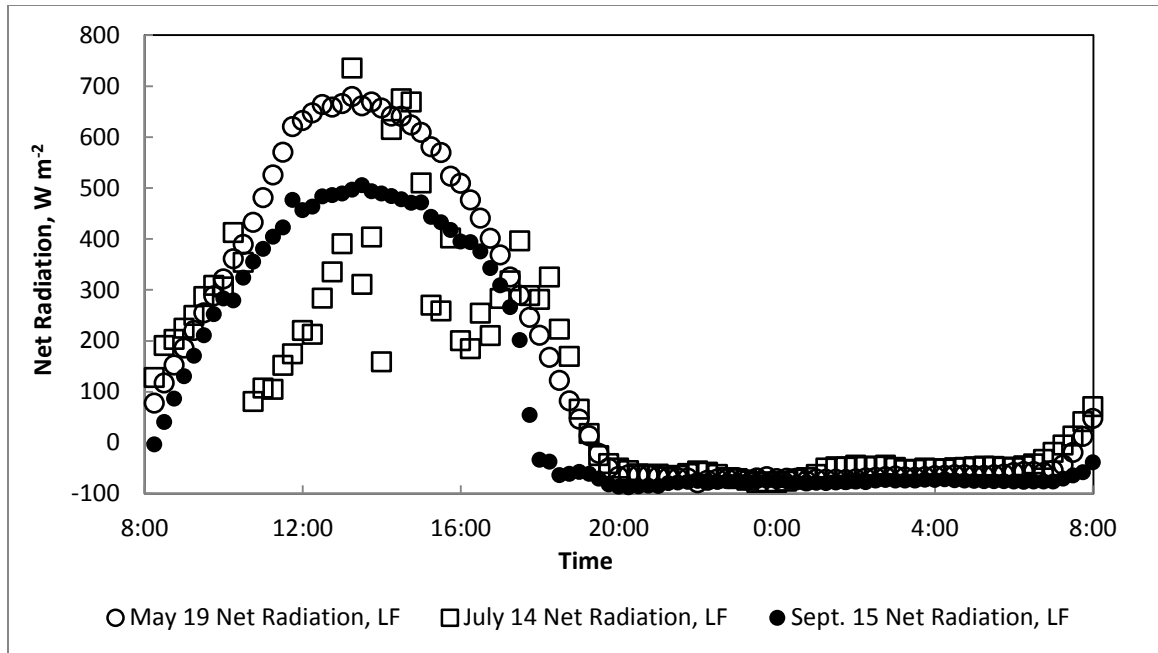

Fig. B4. Key soil conditions spanning 8:00am July 14 to 8:00am July 15, 2012

35

Fig. B5. Key atmospheric conditions spanning 8:00am Sept. 15 to 8:00am Sept. 15, 2012.

Fig. B6. Key soil conditions spanning 8:00am Sept. 15 to 8:00am Sept. 15, 2012

36

Fig. B7. Net Radiation over LF on nights with chamber runs.

References

Allen, R.G., Pereira, L.S., Raes, D., Smith, M., 1998. FAO Irrigation and Drainage Paper No. 56. BERNAN Assoc. Lanham, MD. 290 pp.

American Society of Civil Engineers, 2005. The ASCE Standardized Reference Evapotranspiration Equation. ASCE, Reston, VA.

Bucci, S.J., Goldstein, G., Meinzer, F.C., Franco, A.C., Campanello, P., Scholz, F.G., 2004. Mechanisms contributing to seasonal homeostasis of minimum leaf water potential and predawn disequilibrium between soil and plant water potential in Neotropical savanna trees. Tree Physicology. 19, 296-304.

Benyon, R.G., 1999. Nighttime water use in an irrigated Eucalyptus grandis plantation. Tree Physiology. 19, 853-859.

Caird, M.A., Richards, J.H., Donovan, L.A., 2007. Nighttime stomatal conductance and transpiration in C_3 and C_4 plants. Plant Physiology. 143, 4-10.

Callander, B.A., Woodhead, T., 1981. Canopy conductance of estate tea in Kenya. Agric. Meteorol. 23, 151-167.

Campbell, G.S., 1977. An Introduction to Environmental Biophysics. Springer-Verlag, New York. 159 p.

Crilley, D.M., Collison, J.W., 2012. Domestic consumptive use and potential groundwater recharge from sewage disposal fields in the East Mountain Area, Bernalillo County, New Mexico. 57th Annual NM Water Conference, NMSU. Aug. 28 2012.

Green, S.R., McNaughton, K.G., Clothier, B.E., 1989. Observations of night-time water use in kiwifruit vines and apple trees. Agric. For. Meteorol. 48, 251-261.

England, C.B., 1963. Water use by several crops in a weighing lysimeters. Agron. J. 55, 239-242.

Iritz, A., Lindroth, A., 1994. Night-time evaporation from a short-rotation willow stand. J. Hydrol. 157, 235-245

Jarvis, P.G., and Mansfield, T.A., 1981. Stomatal physiology. Cambridge University Press, Cambridge, UK. 295

Livingston, N.J., Black, T.A., 1987. Stomatal characteristics and transpiration of three species of conifer seedlings planted on high elevation south-facing clear-cut. Can. J. Forest Res. 17 (10), 1273-1282.

Lowe, P.R., 1977. An approximating polynomial for the computation of saturation vapor pressure. J. Appl. Meteorol. 16 (1), 100-103.

McNaughton, K.G., Jarvis, P.G., 1983. Predicting effects of vegetation changes on transpiration and evaporation. Water deficits and plant growth. Academic Press, New York. 7, 1-47.

Monteith, J.L., 1965. Evaporation and environment. In: Fogg,G.E. (Ed.), The State and Movement of Water in Living Organisms. Symposium of the Society for Experimental Biology, vol. 19. Academic Press, New York, pp. 205-234.

Nash, J.E., Sutcliffe, J.V., 1970. River flow forecasting through conceptual models: part I-A discussion of principles. J. Hydrol. 10, 282-290.

Peel, M.C., Finlayson, B.L., McMahon, T.A., 2007. Updated world map of the Köppen-Geiger climate classification. Hydrol. Earth Syst. Sci. 11, 1633-1644.

Rosenberg, N.J. 1969. Seasonal patterns in evapotranspiration by irrigated alfalfa in the central Great Plains. Agron. J. 61, 879-886.

Schuepp, P.H., LeClerc, M.Y., Macpherson, J.I., Desjardins, R.L., 1990. Footprint prediction of scalar fluxes from analytical solutions of the diffusion equation. Boundary-Layer Meteorol. 50, 355-373.

Shuttleworth, W.J., Wallace, J.S., 1985. Evaporation from sparse crops – an energy combination theory. Quart. J. Royal Meteorol. Soc. 111, 839-855.

Snyder, K.A., Richards, J.H., Donovan, L.A., 2003. Night-time conductance in C_3 and C_4 species: do plants lose water at night? J. Experimental Botany. 54, 861-865.

Stannard, D.I., 1988. Use of a hemispherical chamber for measurement of evapotranspiration. Open File Report 88-452. USGS, Washington, DC.

Stannard, D.I., 1993. Comparison of Penman-Monteith, Shuttleworth-Wallace, and modified Priestly-Taylor evapotranspiration models for wildland vegetation in semiarid rangeland. Water Resour. Res. 29, 1379-1392.

Stannard, D.I., 1997. A theoretically based determination of Bowen-ratio fetch requirements. Boundary-Layer Meteorol. 83, 375-406.

Stannard, D.I., Weltz, M.A.,2006. Partitioning evapotranspiration in sparsely vegetated rangeland using a portable chamber. Water Resour. Res. 42, W02413. doi:10.1029/2005WR004251.

Stannard, D.I., Paul, W.T., Laws, R., Poeter, E.P., 2010. Consumptive use and resulting leach-field water budget of a mountain residence. J. of Hydrol. 388, 335-349.

Stewart, J.B., 1988. Modeling surface conductance of pine forest. Agric. Forest Meteorol. 43, 19-35.

Stewart, J.B., Verma, S.B., 1992. Comparison of surface fluxes and conductances at two contrasting sites within the FIFE area. J. Geophys. Res. 97, 18623-18628.

Sugita, M., Brutsaert, W., 1991. Daily evaporation over a region from lower boundary layer profiles measured with radiosondes. Water Resour. Res. 27, 747-752.

Whitley, R., Medlyn, B., Zeppel, M., Macinnis-Ng, C., Eamus, D., 2009. Comparing the Penman-Monteith equation and a modified Jarvis-Stewart model with an artificial neural network to estimate stand-scale transpiration and canopy conductance. J. Hydrol. 373, 256-266.

WRCC, 2013. Western Regional Climate Center. Sandia Park, New Mexico (298015). < http://www.wrcc.dri.edu/>.